Nonlinear lattice models for biopolymers: Dynamical coupling to a ionic cloud and application to actin filaments

Cynthia Ferreira, Guillaume James, Michel Peyrard

NONLINEAR LATTICE MODELS FOR BIOPOLYMERS: DYNAMICAL COUPLING TO A IONIC CLOUD AND APPLICATION TO ACTIN FILAMENTS

Cynthia Ferreira

Institut de Mathématiques de Toulouse (UMR 5219)
Département de Mathématiques, INSA-Toulouse
135 avenue de Rangueil, 31077 Toulouse Cedex 4, France

Guillaume James

Laboratoire Jean Kuntzmann, Université de Grenoble and CNRS
BP 53, 38041 Grenoble Cedex 9, France

Michel Peyrard

Laboratoire de Physique, Ecole Normale Supérieure de Lyon
46 allée d'Italie, 69364 Lyon Cedex 07, France

Abstract. This paper is a first attempt to derive a qualitatively simple model coupling the dynamics of a charged biopolymer and its diffuse cloud of counterions. We consider here the case of a single actin filament. A zig-zag chain model introduced by Zolotaryuk et al [28] is used to represent the actin helix, and calibrated using experimental data on the stiffness constant of actin. Starting from the continuum drift-diffusion model describing counterion dynamics, we derive a discrete damped diffusion equation for the quantity of ionic charges in a one-dimensional grid along actin. The actin and ionic cloud models are coupled via electrostatic effects. Numerical simulations of the coupled system show that mechanical waves propagating along the polymer can generate charge density waves with intensities in the pA range, in agreement with experimental measurements of ionic currents along actin.

1. **Introduction.** Biopolymers can exhibit a variety of complex dynamical behaviors, such as structural transitions in proteins [11] or the breathing of base pairs in DNA [19]. Simulating such phenomena with all-atom models remains a formidable task, due to the large number of degrees of freedom involved and the multiple time scales generated by the dynamics. In addition, realistic models should take into account the effects of the surrounding solvent, which consists in water molecules and ions that greatly influence the physical properties and dynamics of biopolymers. Interestingly, nontrivial dynamical phenomena also occur in the ionic clouds that condense around charged biopolymers. More precisely, experiments performed by

2000 *Mathematics Subject Classification.* Primary: 92B99, 74J30, 70F99, 35Q99; Secondary: 74J35.

Key words and phrases. Biopolymer dynamics, actin filament, nonlinear lattice, dynamical coupling to condensed ions, drift-diffusion model, soliton propagation, charge density waves.

Lin and Cantiello have revealed that ionic signals can propagate inside the ionic cloud surrounding actin filaments [14].

To analyze the dynamics of biopolymers, an alternative to full molecular simulations is the use of simplified lattice models which only retain a small number of essential degrees of freedom per monomer and the main geometrical characteristics of the molecular chain. Despite their relative simplicity, such models qualitatively reproduce experimental observations in different contexts such as DNA breathing [20] or vibrationnal self-trapping in α-helices [7].

In most cases, previous lattice models for biopolymers have separately studied on the one side the vibrational and conformational dynamics (see e.g. [19, 27, 24] in the case of DNA), and on the other side the dynamics of condensed ionic charges [13, 26, 23]. However, since the frequency spectrum of internal motions in biopolymers is very large (ranging from picosecond to millisecond periods), a dynamical coupling between slow internal motions and ionic charges may occur and produce interesting phenomena. Along this direction, Perepelytsya and Volkov have introduced a lattice model coupling the vibrational dynamics of DNA and some of its counterions directly bound to phosphate groups (see [18] and references therein). Their model reproduces a ion-phosphate mode detected in experiments [4], and shows that heavy counterions Cs^+ have an effect on the internal vibrations of DNA. However, their analysis is restricted to alkaline metal ions bound to phosphate groups, treated as a lattice of point charges, and does not take into account the more diffuse ionic cloud surrounding DNA. This other group of ions is usually described by continuum models [8, 9], and it is a challenging task to derive a tractable model that would simultaneously encompass the continuum counterion dynamics and the discrete biopolymer dynamics.

The present paper is a first attempt along this direction. The polymer itself is described by a nonlinear lattice introduced by Zolotaryuk et al consisting in a zig-zag chain [28]. In addition, the polymer is embedded in a ionic cloud divided into fixed cells with averaged charge densities, and the resulting sequence of charge densities satisfies a discrete damped diffusion equation. Both models are nonlinearly coupled via electrostatic effects.

Our contribution consists in three different results. Firstly, we calibrate the mechanical model of Zolotaryuk et al in the case of actin polymers, using available experimental data for the stretching of actin filaments [12, 15]. Secondly, starting from the continuum drift-diffusion model for ionic charge densities [2], we derive a spatially averaged lattice model describing charge densities that is coupled to the above mechanical lattice. Our lattice model for charges is thus derived from first principles, and differs from previous models based on physical assumptions that were not completely justified. Indeed, previous models assumed an analogy between actin and a nonlinear transmission line resulting in a KdV equation for ionic signals [13], the existence of an induction effect resulting from the possible helical motion of charges around the polymer, and a formally introduced nonlinear capacitance effect [26, 23]. Thirdly, we numerically compute the amplitude of charge density waves resulting from an initial localized compression of the polymer. The currents we obtain under low ionic strength conditions lie in the pA range, which is consistent with intensities of ionic signals measured in experiments [14]. In addition we show that compression solitons propagating along the polymer can generate a localized ionic wave in the pA range, propagating steadily with almost no dispersion (the principle of this phenomenon is depicted in figure 1). This phenomenon could

have interesting biological implications since ionic signals play an important role in cellular activities.

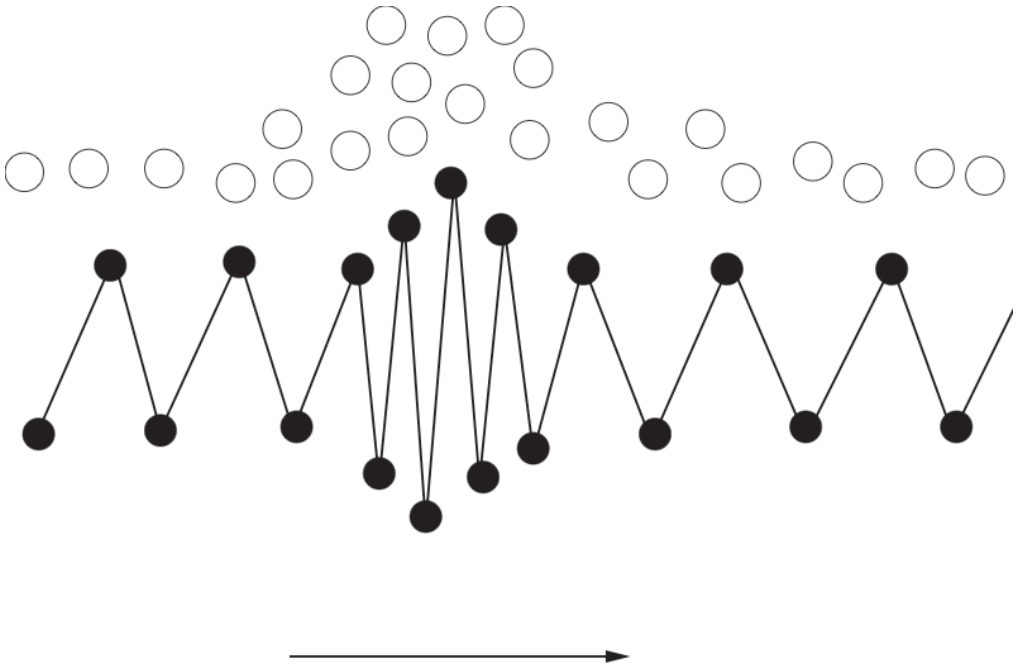

FIGURE 1. Schematic representation of a compression soliton propagating along a biopolymer, and accompanied by a localized charge density wave in the cloud of condensed counterions. Black circles represent surface charges on the polymer, and white circles denote counterions in solution.

This work is of course preliminary, in particular because the description of the electrostatic coupling between the surface charges on the polymer and the condensed counterions is oversimplified. However, it yields physically realistic current intensities despite its great simplicity, and provides a general methodology to couple polymer and charge dynamics that will serve as a basis for a more realistic modelling.

The outline of the paper is as follows. The zig-zag chain model is described in section 2 and calibrated in section 3. In section 4 we establish the lattice model for ionic charges, and couple both models in section 5. Section 6 presents numerical simulations of charge density waves generated by a local compression of the polymer. Section 7 sums up our main results, highlights different directions in which the model must be improved and lists some interesting problems that remain to be examined.

2. **Equations of motion of actin monomers.**

We begin by describing a very simplified model of the geometry of actin and giving the equations of motion of its monomers.

2.1. **Lattice model for an isolated actin filament.**

The actin filament can be represented by a simple helix of pitch $l \approx 5.9$ nm or by a double helix with 72 nm pitch [5, 10]. The helix diameter is $hl \approx 7.5$ nm. We approximate the simple helix by a very simplified planar zig-zag chain model introduced in reference [28], where each monomer is treated as a material point (see figure 2). The distance between first neighbors on the helix is then $a = l(h^2 + 1/4)^{1/2}$. The different types of interactions between monomers (e.g. covalent bonds, hydrogen bonds, electrostatic

forces, contacts interactions) are incorporated in effective potentials. Electrostatic interactions are significant in view of recent results on the distribution of surface charges on actin filaments [1]. Indeed, each actin monomer has a protuberance that is heavily charged ($-10\,e$, e denoting the elementary charge) compared to the remainder of the monomer on which positive and negative charges almost compensate (the total charge of the monomer is $-11\,e$). As a result, a cloud of positive counterions condenses around the actin filament, forming the Debye layer. We include therefore in the equations of motion of monomers an electrostatic force due to this ionic cloud.

We note M_n the nth actin monomer. When n is odd, the monomer M_n is represented by a point of cartesian coordinates $(x_n + nl/2, y_n - lh/2)$. If n is even, M_n is represented by a point of coordinates $(x_n + nl/2, -y_n + lh/2)$. We note $d_{m,n}$ the distance between the monomers M_m and M_n, which is given by

$$d_{m,n}^2 = (x_n - x_m + (n-m)l/2)^2 + (y_n + y_m - lh)^2, \text{ if } (n-m) \text{ is odd,} \quad (1)$$

$$d_{m,n}^2 = (x_n - x_m + (n-m)l/2)^2 + (y_n - y_m)^2, \text{ if } (n-m) \text{ is even.} \quad (2)$$

The potential energy resulting from monomer interactions is given by

$$W = \sum_n (V(d_{n,n+2}) + U(d_{n,n+1})), \quad (3)$$

where U and V are effective potentials describing interactions between first and second neighbors respectively (see figure 2). We set

$$U(x) = \frac{\bar{k}}{2}(x - \bar{a})^2, \quad V(x) = \frac{\bar{k}}{2}(x - \bar{l})^2, \quad (4)$$

where the potentials are written in terms of the small deviations around the structure in the absence of the ionic cloud. The pitch $\bar{l}$ and diameter $\bar{l}\,\bar{h}$ in the absence of counterions will be computed in section 3, and $\bar{a} = \bar{l}(\bar{h}^2 + 1/4)^{1/2}$ is the distance between first neighbors on the chain. The parameter $\bar{k}$ will be deduced from experimental data on actin stiffness (see section 3).

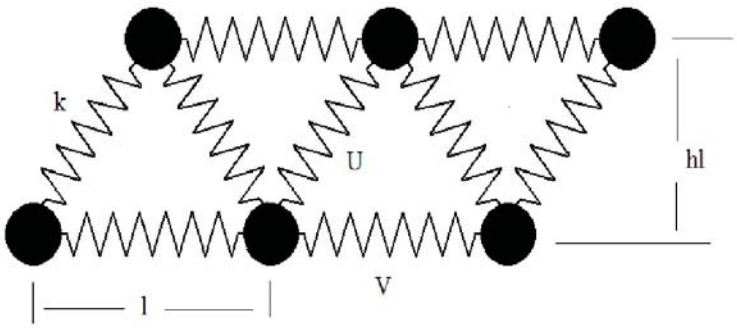

FIGURE 2. Schematic representation of a zig-zag molecular chain.

2.2. **Inclusion of an electrostatic force due to the ionic cloud.** We derive here a very crude approximation of the electrostatic force exerted by the ionic cloud on a given actin monomer. A important parameter is the Debye length κ^{-1} defined by

$$\kappa^2 = \frac{2e^2 n_0}{\epsilon k_B T} \quad (5)$$

where n_0 is the concentration of monovalent ions far from actin, $\epsilon = 7,08.10^{-10}$ USI is the solvent permittivity, $k_B = 1,38.10^{-23}$ J.K^{-1} the Boltzmann constant and T the temperature. The Debye length characterizes the thickness of the diffuse layer of counterions that is formed around the polymer.

Each monomer carries one negative charge $-q$ with $q = 11e$. The electrostatic force exerted on a given monomer by the ionic cloud is estimated in a simple way, assimilating the nth monomer to a point charge $-q$ located at M_n and the surrounding Debye layer to an uniform distribution of charges contained in a half-sphere of radius κ^{-1} around M_n. This rough approximation only takes into account the electrostatic interactions between each monomer and the cloud of counterions in its immediate vicinity, and yields an electrostatic force normal to the chain. We note $(0, g_{2k+1})$ the components of the electrostatic force applied to M_{2k+1} and $(0, -g_{2k})$ those of the force applied to M_{2k}. Denoting by $\widetilde{Q}_n$ the total ionic charge in the Debye layer around M_n, we have

$$g_n = \frac{-3\kappa^2}{16\pi\epsilon} q\widetilde{Q}_n. \tag{6}$$

When the layer of ions and actin are at equilibrium, we have in particular $\widetilde{Q}_n = q$ and $g_n = g_e$ with

$$g_e = \frac{-3\kappa^2}{16\pi\epsilon} q^2. \tag{7}$$

Note that g_e depends on the concentration of ions away from actin. If the ion concentration is $n_0 = c$ mM.l^{-1}, we have at 22°C

$$g_e \approx -2.79\, c \text{ pN} . \tag{8}$$

The equations of motion of the monomers are given by

$$\begin{aligned} M\frac{d^2x_n}{dt^2} &= -\frac{\partial W}{\partial x_n}, \\ M\frac{d^2y_n}{dt^2} &= -\frac{\partial W}{\partial y_n} + g_n \end{aligned} \tag{9}$$

where $M \approx 7,18.10^{-23}$ kg is the mass of one actin monomer. Note that system (9) is nonlinear although potentials U, V in (3) are harmonic, due to geometric nonlinearities.

3. **Calibration of the actin model.** Experiments [12, 15] on the stiffness constant of an actin filament are a good starting point to calibrate our model from experimental data. These works study the elongation δL of a filament under an external force f applied to one end. The stiffness constant $K = f'(\delta L)$ is found almost constant for strong or moderate constraints. However, K decreases sharply with δL when the external force lies below a certain threshold. In this regime, actin behaves like a semi-flexible polymer that undulates as a result of thermal fluctuations and the nonlinear relation giving K can be described using a worm-like chain model [15, 16]. This regime is not correctly described by our model in which we consider a zig-zag chain whose axis is straight when the chain is at rest. Therefore, we restrict ourselves to the parameter regimes for which the stiffness constant of actin remains almost constant.

We consider a filament of $2N + 1$ monomers $M_0, ..., M_{2N}$. The monomer M_0 is kept fixed ($x_0 = 0$) while an external force f is exerted on M_{2N} in the axial direction. To evaluate actin stiffness from our model we consider the case when N

is large and neglect boundary effects, i.e. we assume that interaction forces and helix parameters are independent of n. We note respectively l_1, $l_1 h_1$ the pitch and diameter of the helix in this configuration. The distance between first neighbors on the chain is then $a_1 = l_1(h_1^2 + 1/4)^{1/2}$. The total filament length is $L = Nl_1$ (we assimilate the chain to a straight filament corresponding to the axis of the helix). The filament length at rest is Nl. The elongation of the filament when applying the force is thus

$$\delta L = N(l_1 - l).$$

In this section we shall compute l_1 as a function of f and the unknown stiffness constant $\bar{k}$ of U, V, and determine the latter by comparison with an experimental stress-strain curve.

The transverse and axial components of the equilibrium equations yield

$$-2\frac{l_1 h_1}{a_1} U'(a_1) = g_e, \tag{10}$$

$$V'(l_1) + \frac{l_1}{2a_1} U'(a_1) = f. \tag{11}$$

Using equation (10) in (11) and expressing a_1 in terms of l_1 and h_1, we get the system of equations

$$-2h_1(h_1^2 + 1/4)^{-1/2} U'(a_1) = g_e, \tag{12}$$

$$l_1(h_1^2 + 1/4)^{1/2} = a_1, \tag{13}$$

$$V'(l_1) - \frac{g_e}{4h_1} = f. \tag{14}$$

With this system one can calculate the pitch l_1 and the diameter $l_1 h_1$ as a function of f and the normal stress g_e (which is fixed by the Debye length). Indeed, since U is harmonic, equations (12), (13) determine a_1, l_1 explicitly as functions of h_1, and then f can be expressed as a function of h_1 using equation (14).

To estimate the model parameters, we consider a concentration of monovalent counterions of 25 mM.l^{-1} corresponding to experiments in [12, 15]. Using (8) we obtain $g_e \approx -69.75$ pN. We consider the reference values $l_0 = 5.9$ nm, $h_0 l_0 = 7.5$ nm, $a_0 = 8.06$ nm for the parameters of the unstretched actin filament ($f = 0$) at this ionic concentration.

The potentials defined in (4) are expressed using parameters $\bar{a}, \bar{l}$ of the chain in the absence of counterions (i.e. for $g_e = 0$), which cannot be directly computed at this stage from the equilibrium equations since $\bar{k}$ is not yet determined. Consequently, it is useful to introduce intermediate parameters

$$\lambda_1 = \bar{k}\,(a_0 - \bar{a}), \quad \lambda_2 = \bar{k}\,(l_0 - \bar{l}) \tag{15}$$

which can be directly computed and correspond to interaction forces between adjacent monomers. Indeed, up to the addition of a constant to potentials U and V, we can write

$$U(x) = \lambda_1(x - a_0) + \frac{\bar{k}}{2}(x - a_0)^2, \quad V(x) = \lambda_2(x - l_0) + \frac{\bar{k}}{2}(x - l_0)^2. \tag{16}$$

Using (16) in (12)-(14) yields

$$\frac{g_e}{4}\left[\lambda_2 + \bar{k}(l_1 - l_0) - f\right]^{-1} = h_1, \tag{17}$$

$$l_1(h_1^2 + 1/4)^{1/2} = a_1, \tag{18}$$

$$2h_1(h_1^2 + 1/4)^{-1/2}\left[\lambda_1 + \bar{k}(a_1 - a_0)\right] = -g_e. \tag{19}$$

For unstretched actin ($f = 0$) one has $a_1 = a_0$, $l_1 = l_0$, $h_1 = h_0$ and one finds

$$\lambda_2 = \frac{g_e}{4h_0}, \quad \lambda_1 = -\frac{g_e}{2h_0}(h_0^2 + 1/4)^{1/2},$$

which yields finally

$$\lambda_1 = 37.48 \text{ pN}, \quad \lambda_2 = -13.73 \text{ pN}.$$

Now we are ready to determine the stiffness constant $\bar{k}$ by adjusting the stress-strain relation resulting from (17)-(19) with an experimental curve. We consider figure 10-a of reference [15], which corresponds to an unstretched filament with length $L_c = 19.1\,\mu\text{m} = Nl_0$. We therefore set $N = 3238$ in our model with $2N + 1$ monomers. In the regime of linear elasticity, experiments yield

$$f \approx \frac{K_a}{L_c}\delta L, \quad \delta L = N(l_1 - l_0), \quad K_a \approx 35.5 \text{ nN}.$$

We recover this result when fixing in (16)

$$\bar{k} = 6\,\text{N.m}^{-1} \approx N\frac{K_a}{L_c}. \tag{20}$$

Indeed, solving system (17)-(19) for (l_1, h_1, a_1) for different values of f, we obtain the filament length Nl_1 represented in figure 3. This graph reproduces very precisely the linear part of figure 10-a of reference [15]. Note that when the concentration of ions in solution varies, the stiffness constant $\bar{k}$ computed with our model remains practically unchanged. Moreover, approximation (20) shows that the contribution of potential U to actin stiffness is negligible.

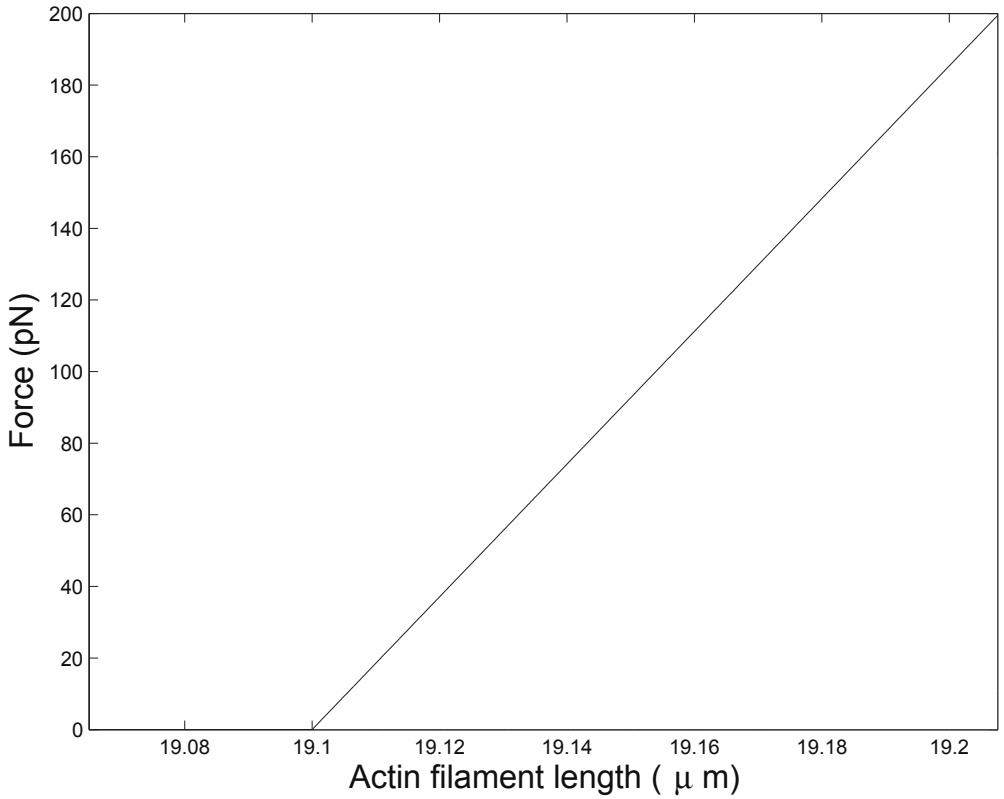

FIGURE 3. Relation between applied stretching force f and filament length Nl_1 for $\bar{k} = 6$ N.m^{-1}, obtained by numerical resolution of (17)-(19). The concentration in monovalent counterions is 25 mM.l^{-1}. The filament length at rest is 19.1 μm ($N = 3238$).

Using (15) and the values of $\lambda_1, \lambda_2, \bar{k}$ previously obtained, we find

$$\bar{a} \approx 8.053\,\text{nm}, \quad \bar{l} \approx 5.902\,\text{nm}, \quad \bar{l}\,\bar{h} = (\bar{a}^2 - \frac{\bar{l}^2}{4})^{1/2} \approx 7.493\,\text{nm},$$

hence the values of $\bar{l}$ and $\bar{l}\,\bar{h}$ are extremely close to those of l_0 and $h_0 l_0$. More generally, it is interesting to study how the pitch l and diameter hl at equilibrium depend on the concentration of ions in solution. For this purpose we numerically solve system (17)-(19) with $f = 0$, which can be rewritten

$$\begin{aligned} h(l - \bar{l}) &= \frac{g_e}{4\bar{k}}, \\ l(h^2 + 1/4)^{1/2} &= a, \\ h(h^2 + 1/4)^{-1/2}(a - \bar{a}) &= -\frac{g_e}{2\bar{k}}. \end{aligned}$$

We obtain only very small variations, at most of the order of 0.1 $\mathring{A}$ for l and 0.4 $\mathring{A}$ for hl, when we change the ionic concentration.

4. **Lattice model for counterion dynamics.** In this section we use the classical drift-diffusion system [2] to derive a lattice model approximating the quantity of ionic charges in fixed cells around actin. This model is coupled with the above chain model because the charge density in the Debye layer depends on the distribution of surface charges along actin, which is a function of monomer positions.

In what follows, in order to analyze the dynamics of the ions in the continuous fluid medium that surrounds actin, we look at the system from a different perspective, at a larger scale. At this level of description we can view the actin filament as a simple cylinder, which carries charges which are distributed in an extended domain around the center of each monomer. Therefore we consider now the actin filament as an infinite cylinder of radius $r_a = lh/2$ and denote by x the axial coordinate. We begin by constructing an equivalent axisymmetric charge distribution $\sigma(t, x)$ associated with monomer positions. The axial coordinate of the center of monomer n is $x_n(t) + nl/2$ and we consider that the surface charge of the monomer is mainly contained in a segment of width $l/2$ around his center [1]. A point with coordinate x belongs to this segment when $|x - x_n(t) - nl/2| < l/4$, i.e. for $|\frac{2(x-x_n(t))}{l} - n| < 1/2$. The modulus of the surface charge density on a monomer (centered at $x = 0$, for l renormalized to 2) is assumed proportional to

$$\chi(x) = \begin{cases} 0, & \text{if} \quad |x| \geq 1/2 \\ 2 - 4|x|, & \text{if} \quad |x| \leq 1/2, \end{cases} \tag{21}$$

(note that $\int_{\mathbb{R}} \chi dx = 1$). The equivalent surface charge distribution associated with polymer positions is then defined by

$$\sigma(t, x) = \frac{1}{2\pi r_a} \frac{-2q}{l} \sum_n \chi[\frac{2(x - x_n(t))}{l} - n]. \tag{22}$$

When actin is at equilibrium ($x_n = 0$), the charge density has period $l/2$ in x and can be written

$$\bar{\sigma}(x) = \frac{1}{2\pi r_a} \frac{-2q}{l} \sum_n \chi(\frac{2x}{l} - n).$$

Integrating on a segment with N monomers we find

$$\int_0^{2\pi} \int_{-l/4}^{(l/4)+(N-1)l/2} \bar{\sigma}\, dx\, r_a\, d\theta = -q\, N.$$

We observe that when $l \approx 0$, $\sigma \approx \frac{-q}{2\pi r_a} \sum_n \delta_{x_n(t)+nl/2}(x)$ and we recover the case of a point charge distribution.

Actin is surrounded by a cloud of counterions which compensates its surface charge. We will now introduce the drift-diffusion model for these ions and make simplifying assumptions leading to an equivalent electrical circuit. In the case of a single ion species, the density of charge $\rho(t, x, r)$ in the Debye layer satisfies [2]

$$\frac{\partial \rho}{\partial t} + \mathrm{div} J = 0, \tag{23}$$

where

$$J = -D\nabla\rho - \rho\mu\nabla\phi, \tag{24}$$

μ denotes the ion mobility, D its diffusion coefficient and ϕ the electric potential in the Debye layer due to ions and surface charges. The potential ϕ satisfies a Poisson equation $\Delta\phi = -\rho/\epsilon$.

We neglect from now the ionic charges situated outside the Debye layer and suppose that the latter compensates the total charge of actin. Furthermore, we divide the Debye layer in an infinity of cylindrical domains defined by

$$\Omega_n = \{(r, \theta, x)/r_a < r < r_a + \kappa^{-1}, a_{n-1} < x < a_n\},$$

with $a_n = \frac{l}{2}(n + \frac{1}{2})$. This discretization is useful for the analysis of the next section, which couples the dynamics of the discrete actin model with that of the ionic cloud. We perform the following approximation in the Debye layer

$$J \approx -D\nabla\rho - \overline{\rho}\mu\nabla\phi. \tag{25}$$

The term $\overline{\rho}\mu$ corresponds to an electrical conductivity averaged in the domain Ω_n when the actin is at rest. This approximation is similar to the one used to establish Ohm's law for electrical circuits, in which the electrical conductivity is assumed constant in each resistance. We fix

$$\overline{\rho} = \frac{2q\kappa}{l\pi(hl + \kappa^{-1})} \tag{26}$$

so that a layer of ions of density $\overline{\rho}$ in Ω_n exactly compensates the charge of monomer n when actin is at rest.

The ionic charge Q_n contained in Ω_n is

$$Q_n = \iiint_{\Omega_n} \rho\, r dr d\theta dx. \tag{27}$$

Integrating (23) over Ω_n, using (25) and taking into account the no-flux boundary conditions $J.\overrightarrow{n} = 0$ at $r = r_a$ and $r = r_a + \kappa^{-1}$, we obtain

$$\begin{aligned} \frac{dQ_n}{dt} &= 2\pi D \int_{r_a}^{r_a+\kappa^{-1}} \left[\frac{\partial \rho}{\partial x}(a_n, r) - \frac{\partial \rho}{\partial x}(a_{n-1}, r)\right] r dr \\ &\quad + 2\pi\mu\overline{\rho} \int_{r_a}^{r_a+\kappa^{-1}} \left[\frac{\partial \phi}{\partial x}(a_n, r) - \frac{\partial \phi}{\partial x}(a_{n-1}, r)\right] r dr \end{aligned} \tag{28}$$

(we omit dependency in t in notations).

Now we approximate each term at the right side of (28). We note that for $l \approx 0$

$$\begin{aligned} Q_{n+1} - 2Q_n + Q_{n-1} &= \iiint_{\Omega_n} \left[\rho(x+\frac{l}{2},r) - 2\rho(x,r) + \rho(x-\frac{l}{2},r)\right] r dr d\theta dx \\ &\approx 2\pi \frac{l^2}{4} \int_{r_a}^{r_a+\kappa^{-1}} \int_{a_{n-1}}^{a_n} \frac{\partial^2 \rho}{\partial x^2}(x,r)\, dx\, r dr \\ &= \pi \frac{l^2}{2} \int_{r_a}^{r_a+\kappa^{-1}} \left[\frac{\partial \rho}{\partial x}(a_n,r) - \frac{\partial \rho}{\partial x}(a_{n-1},r)\right] r dr. \end{aligned}$$

Therefore,

$$2\pi D \int_{r_a}^{r_a+\kappa^{-1}} \left[\frac{\partial \rho}{\partial x}(a_n,r) - \frac{\partial \rho}{\partial x}(a_{n-1},r)\right] r dr \approx \frac{4D}{l^2}(Q_{n+1} - 2Q_n + Q_{n-1}). \quad (29)$$

Also, using the Gauss theorem

$$\iint_{\partial\Omega_n} -\nabla\phi.\overrightarrow{n}\, dS = \frac{Q_n}{\epsilon},$$

with the boundary conditions

$$\frac{\partial \phi}{\partial r}(x,r_a) = -\frac{\sigma}{\epsilon}, \quad \frac{\partial \phi}{\partial r}(x,r_a+\kappa^{-1}) = 0,$$

we get

$$2\pi\mu\overline{\rho} \int_{r_a}^{r_a+\kappa^{-1}} \left[\frac{\partial \phi}{\partial x}(a_n,r) - \frac{\partial \phi}{\partial x}(a_{n-1},r)\right] r dr = -\frac{\mu}{\epsilon}\overline{\rho}(Q_n + 2\pi r_a \int_{a_{n-1}}^{a_n} \sigma dx). \quad (30)$$

Using (29) and (30) in (28) we obtain finally

$$\frac{dQ_n}{dt} = \frac{4D}{l^2}(Q_{n+1} - 2Q_n + Q_{n-1}) - \frac{\mu}{\epsilon}\overline{\rho}(Q_n + 2\pi r_a \int_{a_{n-1}}^{a_n} \sigma dx). \quad (31)$$

Note that if x_n is independent of n (i.e. actin is simply translated) we have

$$2\pi r_a \int_{a_{n-1}}^{a_n} \sigma dx = -q$$

and $Q_n = q$ is an equilibrium solution of (31).

We note in the sequel $Q_n = q + q_n$. Using definition (22), problem (31) can be rewritten

$$\frac{dq_n}{dt} = \frac{4D}{l^2}(q_{n+1} - 2q_n + q_{n-1}) - \frac{\mu}{\epsilon}\overline{\rho}\big(q_n + q - q\sum_p \big[\int_{-\frac{1}{2}+p}^{\frac{1}{2}+p} \chi(x - \frac{2}{l}x_{n-p})dx\big]\big). \quad (32)$$

To simplify equation (32) we assume small monomer displacements with $|x_n| < l/4$, so that the center of monomer n (for which $x = x_n(t) + nl/2$) is inside the domain Ω_n at $r = r_a$. In equation (32), the coupling term involving monomer displacements is then reduced to a sum of three terms. Then (after a change of variables in the integrals) problem (32) can be rewritten

$$\frac{dq_n}{dt} = \frac{4D}{l^2}(q_{n+1} - 2q_n + q_{n-1}) - \frac{\mu}{\epsilon}\overline{\rho}q_n + q\frac{\mu}{\epsilon}\overline{\rho}(F(-x_{n+1}) - F(x_n) - F(-x_n) + F(x_{n-1})) \quad (33)$$

with

$$F(x) = \int_{\frac{1}{2}-\frac{2}{l}x}^{\frac{1}{2}} \chi(y)dy. \quad (34)$$

We recall that the function χ appearing in (34) is defined by (21). Note that to maintain the conservation of charge in (33) we are restricted to initial conditions satisfying $\sum_n q_n = 0$, i.e. to neutral electrical systems.

5. **Coupled model for actin and condensed counterions.** In this section we sum up the main features of the two models established in the previous sections, precise certains points concerning their coupling and briefly compare them to existing models.

We consider harmonic interaction potentials U and V corresponding to nearest neighbors and next nearest neighbors interactions along the chain, defined by

$$\begin{aligned} U(x) &= \frac{\bar{k}}{2}(x-\bar{a})^2, \quad V(x) = \frac{\bar{k}}{2}(x-\bar{l})^2, \\ \bar{k} &= 6\,\mathrm{N.m}^{-1}, \quad \bar{l} \approx 5.9\,\mathrm{nm}, \quad \bar{a} \approx 8.1\,\mathrm{nm}. \end{aligned}$$

We fix a Debye length κ^{-1} and consider the characteristic lengths l, hl, a of actin at equilibrium determined by the system

$$h(l-\bar{l}) = -\frac{3\kappa^2}{64\pi\bar{k}\epsilon}q^2, \tag{35}$$

$$l(h^2+1/4)^{1/2} = a, \tag{36}$$

$$h(h^2+1/4)^{-1/2}(a-\bar{a}) = \frac{3\kappa^2}{32\pi\bar{k}\epsilon}q^2. \tag{37}$$

The dependency of l, h and a with respect to the Debye length is in fact negligible.

We consider the case of small monomer displacements with $|x_n| < l/4$. In that case, the center of monomer M_n is located within the domain Ω_n at $r = r_a$, but the monomer also intersects the cell Ω_{n+1} or Ω_{n-1}. The amount of charge $\widetilde{Q}_n$ condensed on M_n depends consequently on the charges Q_n contained in the fixed cells $\Omega_n, \Omega_{n\pm1}$ and on the displacements x_n. We determine $\widetilde{Q}_n$ with the following simple expression

$$\widetilde{Q}_n(x_n, Q_{n-1}, Q_n, Q_{n+1}) = \begin{cases} \alpha Q_{n+1} + (1-\alpha)Q_n \text{ if } x_n = \frac{l}{2}(n+\alpha),\ \alpha \in [0, \frac{1}{2}], \\ \\ \alpha Q_{n-1} + (1-\alpha)Q_n \text{ if } x_n = \frac{l}{2}(n-\alpha),\ \alpha \in [0, \frac{1}{2}]. \end{cases}$$

The equations of motion of the monomers read

$$\begin{aligned} M\frac{d^2x_n}{dt^2} &= -\frac{\partial W_n}{\partial x_n}, \\ M\frac{d^2y_n}{dt^2} &= -\frac{\partial W_n}{\partial y_n} - \frac{3\kappa^2}{16\pi\epsilon}q\widetilde{Q}_n(x_n, Q_{n-1}, Q_n, Q_{n+1}) \end{aligned} \tag{38}$$

where

$$W_n = V(d_{n-2,n}) + V(d_{n,n+2}) + U(d_{n-1,n}) + U(d_{n,n+1}).$$

We set $M \approx 7,18.10^{-23}$ kg and distances $d_{m,n}$ are defined in equations (1)-(2). The ionic charges $Q_n = q + q_n$ in the cells Ω_n partitioning the Debye layer satisfy

$$\frac{dq_n}{dt} = \frac{4D}{l^2}(q_{n+1}-2q_n+q_{n-1}) - \frac{\mu}{\epsilon}\overline{\rho}q_n + q\frac{\mu}{\epsilon}\overline{\rho}(F(-x_{n+1})-F(x_n)-F(-x_n)+F(x_{n-1})), \tag{39}$$

where the nonlinearity F is defined by (34). Constants μ, D denote respectively the mobility and diffusion coefficient of the counterion species, and $\overline{\rho}$ is determined by the Debye length via equation (26).

System (38)-(39) has a family of equilibria defined by $x_n = x_0$ (x_0 arbitrary constant), $y_n = 0$, $\dot{x}_n = 0$, $\dot{y}_n = 0$ and $q_n = 0$, corresponding to translations of the chain at rest.

It is interesting to compare the dispersion relation of the model (38) with $\kappa = 0$ (uncoupled limit) to that obtained by ben-Avraham and Tirion [3] with a much more realistic three-dimensional model of actin. Model (38) linearized at the ground state has acoustic and optical modes whose dispersion relations are shown in reference [28] (figure 2-b p.3886). The acoustic branch of this figure reproduces qualitatively the acoustic branch obtained in [3] (figure 3 p.1236, branch noted "a"). The optical branch of [28] also reproduces an optical branch of [3] (branch marked "d" in figure 3 p.1236). We will now compare these branches in a more quantitative way. We first compare the optical branches. Linearizing equation (38) and looking for solutions in the form of normal modes whose components are proportional to $e^{i(\frac{k}{2}n-\omega t)}$, Zolotaryuk et al obtain for $k \approx 0$ the dispersion relation

$$\omega_{opt} = 10^{12}(0,73 - \frac{k^2}{100})$$

when ω_{opt} is expressed in s^{-1}. The model of ben-Avraham and Tirion gives $\omega_{opt} = 0,35.10^{12}\ \mathrm{s}^{-1}$ when $k = 0$, which is of the same order of magnitude. The comparison is quite satisfactory and it should be possible to match even more these two results by allocating nonequal stiffness constants to the potentials U and V in our model. Moreover, the slope at the origin on the acoustic branch gives the longitudinal sound velocity c_g in actin. Using equation (53) of [28] we get $c_g \approx 1705\ \mathrm{m.s}^{-1}$. The value obtained by ben-Avraham and Tirion is $c_g \approx 1310\ \mathrm{m.s}^{-1}$. Both results are again of the same order of magnitude. These comparisons with the more realistic model [3] are therefore quite good given the simplicity of the zig-zag chain model.

Concerning ionic charges, equation (39) without the configurational coupling terms consists in a linear and spatially discrete damped diffusion equation. The nonlinearity resides therefore in the coupling to longitudinal actin deformation, and in the nonlinear dynamics of actin itself which influences the surrounding ionic charges. Previously derived equivalent circuit models for actin are of a different type, including an inertial term accouting for an induction effect, as well as a nonlinear capacitance effect [26].

6. **Numerical simulations.** In this section we perform some numerical simulations of the coupled system actin-ionic cloud (38)-(39) introduced in section 5. Simulations are done for a chain of 1000 monomers with periodic boundary conditions. We consider the case of K^+ counterions with mobility $\mu = 7,62.10^{-8}\,\mathrm{m}^2(\mathrm{V.s})^{-1}$. Their diffusion coefficient is $D = 1,96.10^{-9}\,\mathrm{m}^2\mathrm{s}^{-1}$ at 25°C. The Debye length is set to $\kappa^{-1} = 10$ nm, which corresponds to low ionic strength experimental conditions considered in reference [14]. The Debye layer is considered initially at equilibrium and the initial conditions taken for the chain are described below.

6.1. **Single monomer compression.** We fix $x_n = l/5$ if $n = 1...499$, $x_{500} = 0$ and $x_n = -l/5$ if $n = 501...1000$. Consequently the bonds between the monomers $499, 500$ and 501 are compressed, which corresponds to a compression of the central monomer at $n = 500$.

Figure 4 shows the system state after a very short time of $1,8.10^{-11}s$. We can see that the chain perturbation gives rise to a localized perturbation of the ionic charges. This initial condition produces two dispersive elastic shock waves that propagate

in opposite directions along the chain. These waves and their dispersive tail (figure 5, top) generate in turn charge density waves (figure 5, bottom). The propagation of these charge density waves is clearly visible on the space-time diagram shown in figure 6. Lastly, figure 7 depicts the temporal evolution of the ionic current at monomer $n = 450$. The main shock is followed by charge density waves with intensities of the order of 1 pA, in agreement with experimental measurements of ionic currents along actin performed by Lin and Cantiello [14].

Note however that ionic currents measured in [14] appear as transient states over tenths of milliseconds, whereas our computations are performed on the ns time scale, which lies well below the experimental resolution available from [14]. The charge density waves we compute here are much faster and excited by elastic waves, whereas the ionic signals observed in [14] result from an initial voltage pulse applied to actin in solution. It is therefore not possible to compare the charge dynamics in both cases, but we can however conclude that the current intensities we obtain are physically realistic.

6.2. **Compression soliton.** Solitons form an interesting class of nonlinear waves due to their ability to transport energy or information over long distances without changing form. Zolotaryuk et al have shown that the zig-zag chain model supports soliton solutions, using both numerical computations and amplitude equations based on multiscale expansions [28] (see also [6, 25]). Such solutions exist in particular in our model with harmonic interaction potentials due to the geometric nonlinearity of the system. Our previous numerical simulations have shown that elastic waves generated by a localized polymer compression can serve as carrier waves for charge density waves. We will now consider an initial condition corresponding to a compression soliton, and show its ability to generate a localized ionic wave with an intensity relevant at the biological scale, propagating steadily with almost no dispersion.

Figure 8 represents an initial condition that generates a compression soliton (velocities are not represented and are chosen such that the soliton propagates rightwise). This initial condition is given by an analytical approximation of the soliton profile computed in reference [28]. As previously the cloud of counterions is chosen initially at rest. As shown by figure 9 (upper plot), the soliton propagates rightwise accompanied by a small dispersion and a much smaller soliton propagating to the left. We attribute these effects to the imperfect initial condition, and to the coupling of the soliton with the charge perturbation generated at the initial stage. The ionic waves produced by the solitons are shown in figure 9 (lower plot). The main soliton generates a charge density wave in the pA range, propagating steadily with almost no dispersion, while the electric signature of the smaller soliton remains negligible.

7. **Conclusion.** We have proposed a new methodology to couple a lattice model for the vibrations of a charged biopolymer and the dynamics of its ionic cloud. We have considered the case of a single actin filament, and used a zig-zag chain model introduced by Zolotaryuk et al [28] to account for the helical structure of actin. We have calibrated this model using experimental data on the stiffness constant of actin filaments [15], and found a good agreement between the optical and acoustic mode frequencies of the zig-zag chain and those of a more realistic three-dimensional model of actin [3]. In addition we have derived a discrete damped diffusion equation for the quantity of surrounding ionic charges, obtained using a drift-diffusion model

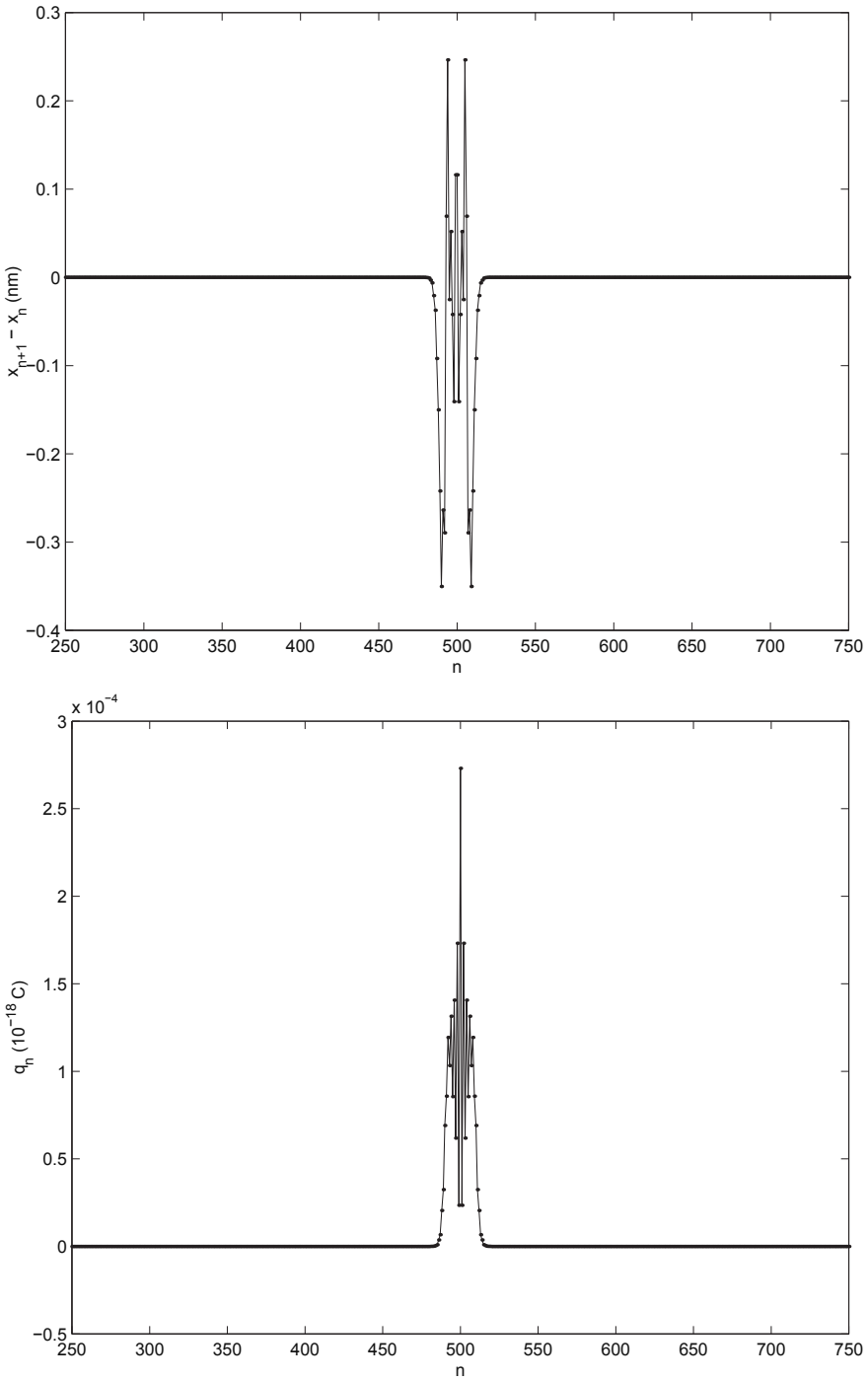

FIGURE 4. State of the system at an early stage ($t = 1,8.10^{-11}s$) after an initial localized compression of the chain (see text). The upper plot gives the variation along the chain of the axial distance between adjacent monomer centers, and the lower plot shows the localized charge perturbation q_n induced in the ionic cloud.

averaged in a one-dimensional grid along actin. The actin and ionic cloud models have been coupled via electrostatic effects. Numerical simulations have shown that mechanical waves propagating along the polymer can generate charge density waves with intensities in the pA range, in agreement with experimental measurements of ionic currents [14].

The challenge of this study was to simultaneously include the discrete character of actin dynamics and the dynamics of the counterions in solvent, which is intrinsically

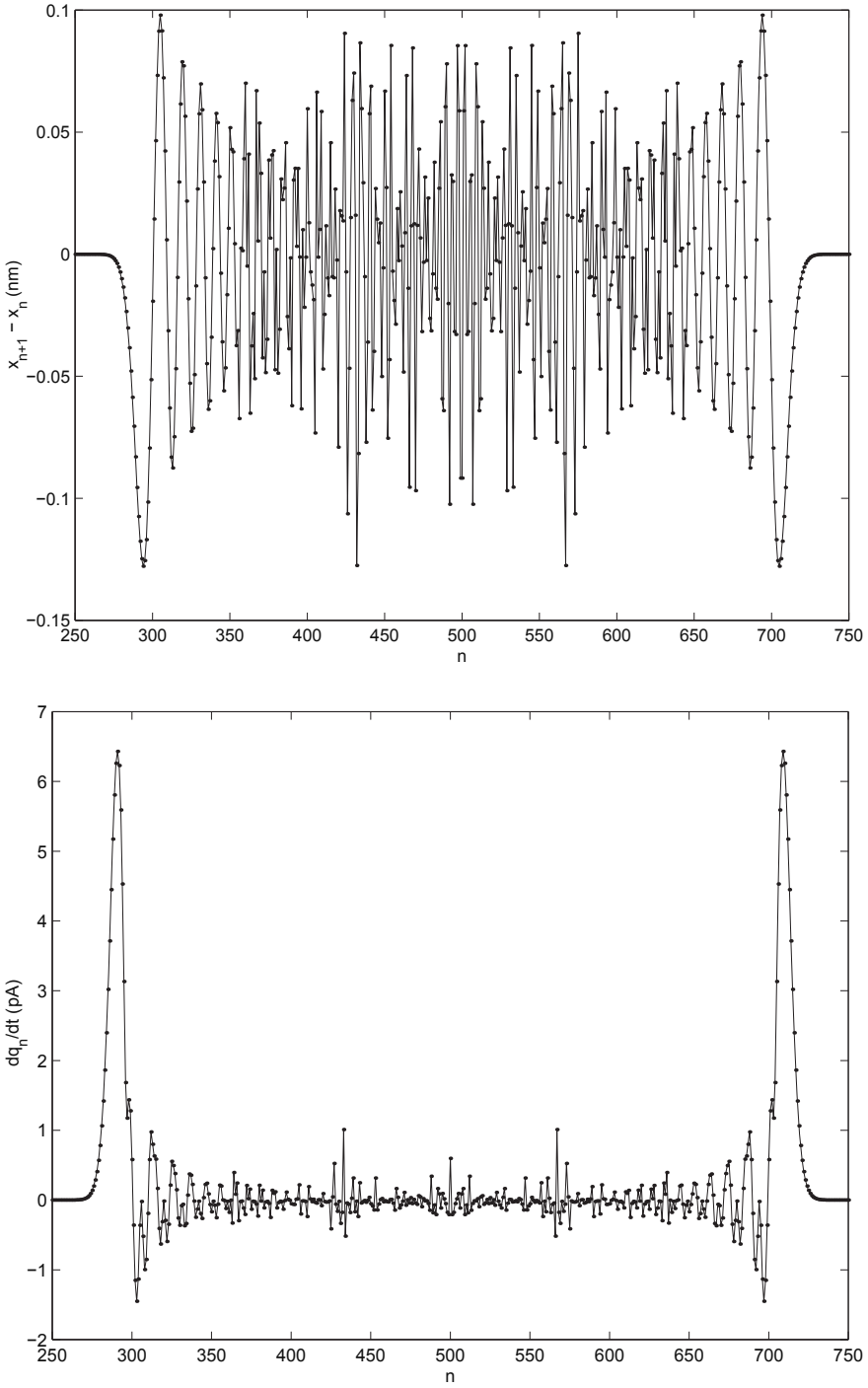

FIGURE 5. Top figure : same plot as figure 4, at a later time $t = 0,36.10^{-9}s$. Two shock waves and their dispersive tail are clearly visible. Bottom figure : current dq_n/dt in the ionic cloud induced by these elastic waves.

continuous. This has been done by dividing the continuous ionic cloud system into domains and determining an equation for the evolution of the charges in these domains. This allowed us to reconcile the discrete and continuous aspects of the system, and to derive a law for their coupled dynamics, but this has been done at the expense of introducing some approximations.

This work will be extended in several directions. Firstly, although the current intensities we obtain with such a simple model are encouraging, our approximation of the electrostatic forces exerted on actin by the solvent is oversimplified. A more

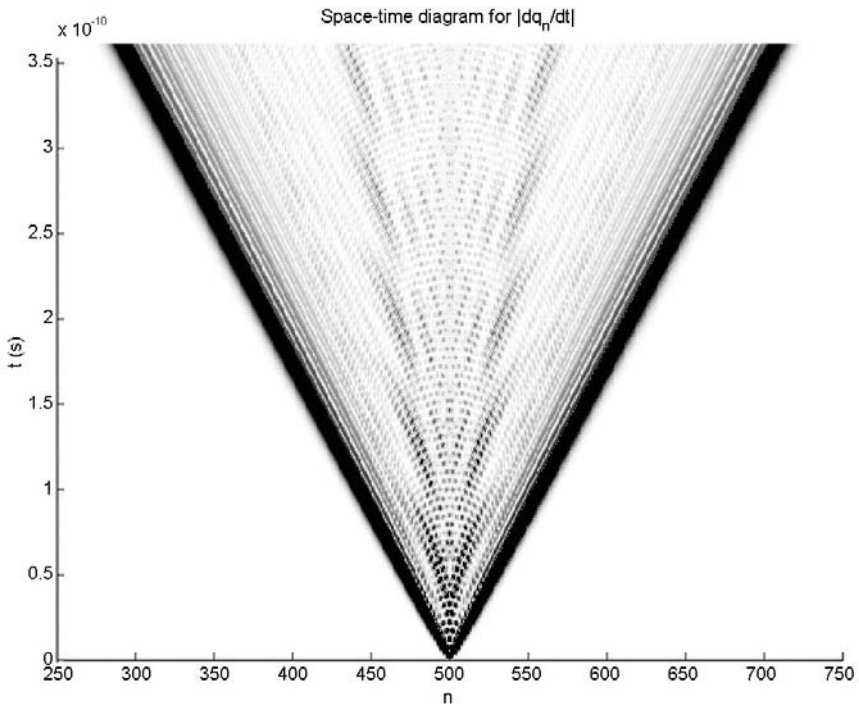

FIGURE 6. Space-time diagram showing $|dq_n/dt|$ in grey levels, for the same initial condition as figure 4. White regions correspond to a vanishing current, and black ones to intensities $> 2{,}5$ pA.

realistic coupling term will be derived using the Poisson-Boltzmann equation as described in reference [9], taking into account dielectric boundary forces that were neglected in our model. In addition a realistic modelling should incorporate the effects of viscous damping and thermal fluctuations due to the solvent.

Secondly, we have focused in this paper on the derivation and calibration of the model, and on the intensity of charge density waves generated by elastic waves. It will now be interesting to investigate the dynamics of the model in more details, and determine in particular if the coupling with surrounding charges could affect the dynamics of the polymer itself.

In addition, our approach could be applied to other charged biopolymers like DNA or microtubules. The dynamics of ionic charges around microtubules can result in interesting phenomena, e.g. an amplification of electrical signals detected in recent experiments [22]. A lattice model for elastic vibrations of microtubules is available [21], and could be coupled to a model for ionic charges similar to ours. This model for charge propagation gives an interesting alternative to existing ones [23] because it relies on the physically well-established drift-diffusion equations.

Lastly, it will be interesting to generalize our approach to include other modes of actin like bending and twisting. In particular, modes acting on a slower timescale may lead to interesting coupling effects with counterion dynamics. This problem could be considered e.g. for torsional motions, which are able to generate transient states that persist for several seconds [17]. Since twisting and stretching modes are coupled, twisting will affect the counterion dynamics via an electrostatic coupling similar to the one described in this paper. In particular, it would be interesting to see if torsion waves could generate charge density waves along actin with periods of the order of a few ms. Electrical signals of this type have been experimentally

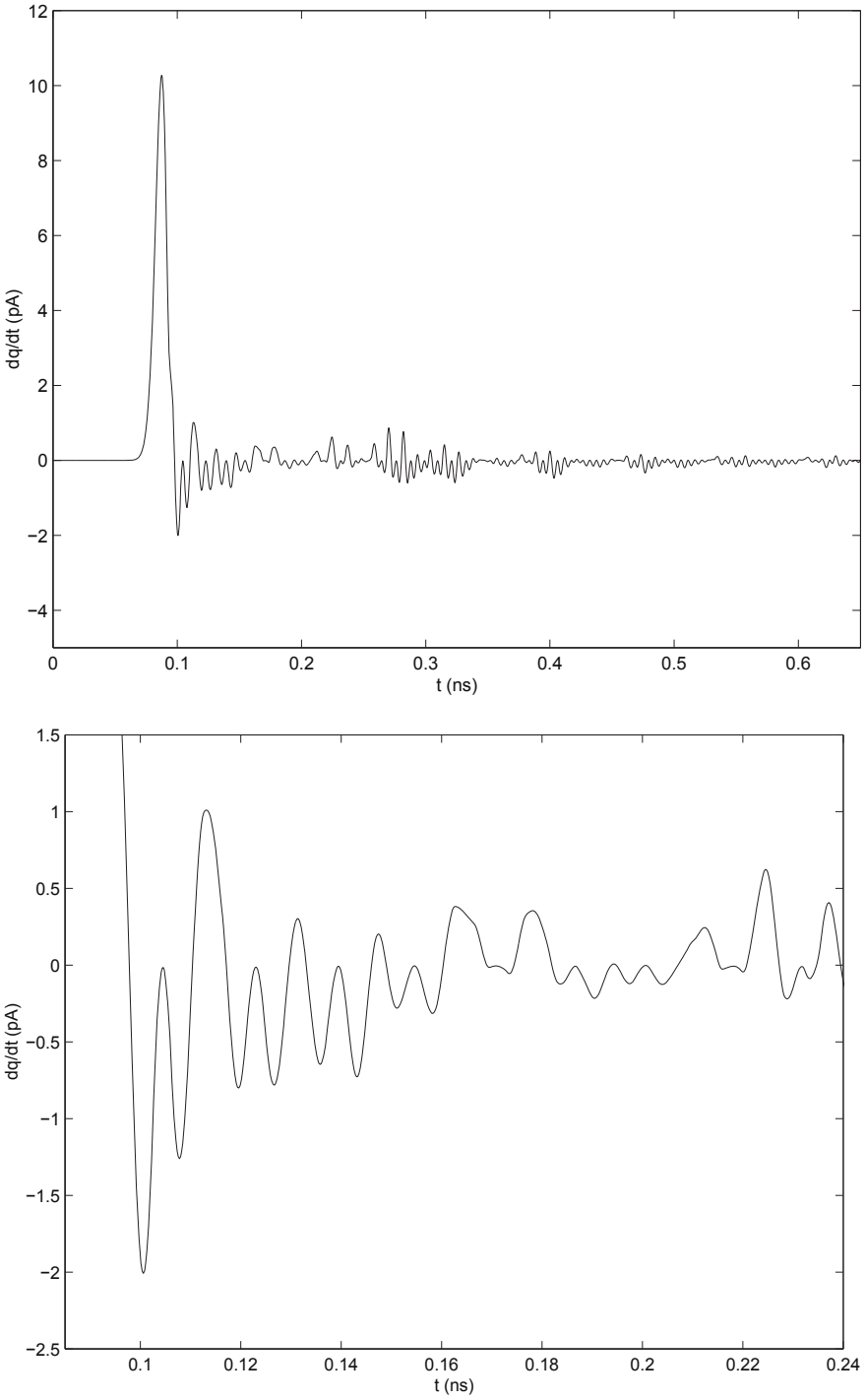

FIGURE 7. Temporal evolution of the current intensity dq_n/dt at monomer $n = 450$, for the same initial condition as figure 4. The bottom figure provides a zoom of the profile after the main shock.

detected by Lin and Cantiello [14], and this phenomenon is still lacking a well-established physical explanation.

Acknowledgments. This work has been supported by the CAPES (Coordenaçao de Aperfeiçoamento de Pessoal de Nivel Superior- Brasil, www.capes.gov.br) and the CNRS program ACI Nouvelles Interfaces des Mathématiques (2004-2007). Stimulating discussions with Naoufel Ben Abdallah, Pierre Degond and Florian Méhats are gratefully acknowledged. The authors thank the referees for useful remarks.

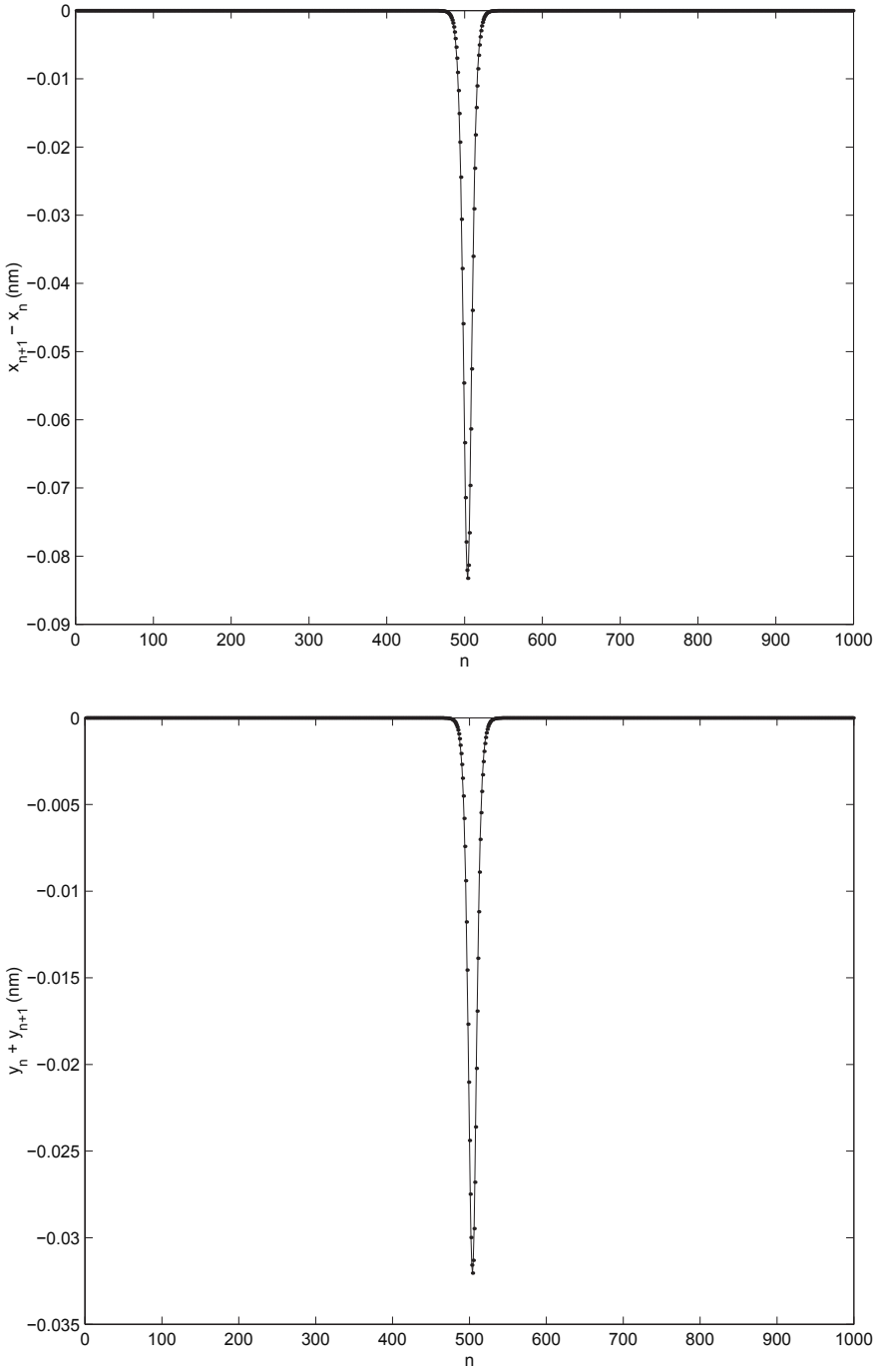

FIGURE 8. Initial horizontal (upper plot) and vertical (lower plot) perturbations of the polymer configuration corresponding to a compression soliton.

REFERENCES

[1] T. E. Angelini, et al., *Counterions between charged polymers exhibit liquid-like organization and dynamics*, Proc. Natl. Acad Sci. USA, **103** (2006), 7962–7967.

[2] N. Ben Abdallah, F. Méhats and N. Vauchelet, *A note on the long time behavior for the drift-diffusion-Poisson system*, C. R. Acad. Sci. Paris Ser. I, **339** (2004), 683–688.

[3] D. ben-Avraham and M. Tirion, *Dynamic and elastic properties of F-actin: A normal mode analysis*, Biophys. J., **68** (1995), 1231–1245.

[4] L. A. Bulavin, S. N. Volkov, S. Yu. Kutuvy and S. M. Perepelytsya, *Observation of the DNA ion-phosphate vibrations*, Proceedings of National Academy of Science of Ukraine, **11** (2007), 69–73, `arXiv:0805.0696v1`.

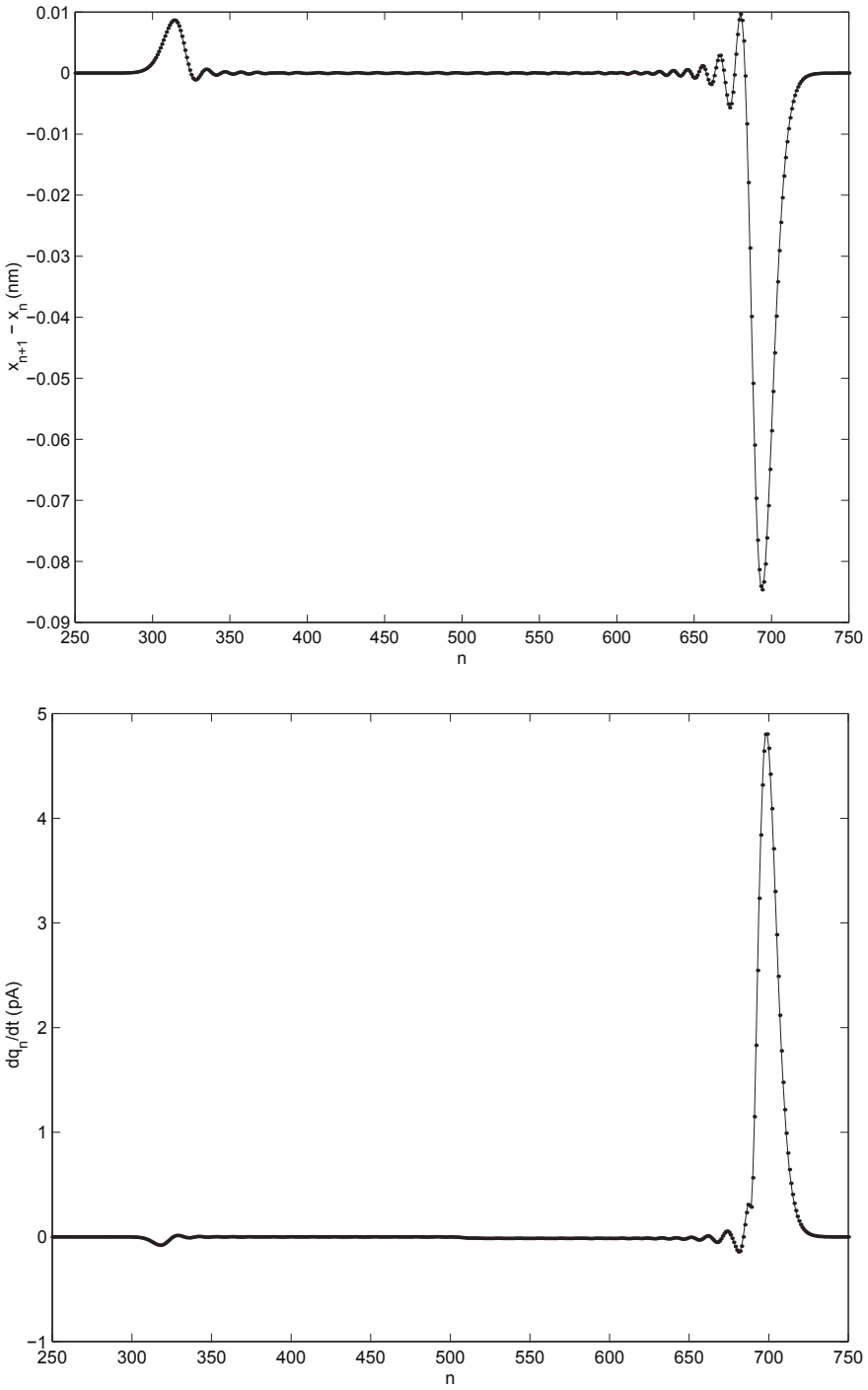

FIGURE 9. Top figure : solitary wave propagating rightwise, generated by the initial perturbation of the chain given in figure 8. The larger soliton is accompanied by a smaller one propagating in the opposite direction. Bottom figure : intensity dq_n/dt of the localized charge density wave generated by the main soliton. Both plots correspond to $t = 0, 33.10^{-9}s$.

[5] M.-F. Carlier, *Actin: Protein structure and filament dynamics*, J. Biol. Chem., **266** (1991), 1–4.

[6] P. L. Christiansen, A. V. Savin and A. V. Zolotaryuk, *Soliton analysis in complex molecular systems: A zig-zag chain*, Journal of Computational Physics, **134** (1997), 108–121.

[7] J. Edler, R. Pfister, V. Pouthier, C. Falvo and P. Hamm, *Direct observation of self-trapped vibrational states in α-helices*, Phys. Rev. Lett., **93** (2004), 106405.

[8] F. Fogolari, P. Zuccato, G. Esposito and P. Viglino, *Biomolecular electrostatics with the linearized Poisson-Boltzmann equation*, Biophys. J., **76** (1999), 1–16.
[9] M. K Gilson, M. E. Davis, B. A. Luty and J. A. McCammon, *Computation of electrostatic forces on solvated molecules using the Poisson-Boltzmann equation*, J. Phys. Chem., **97** (1993), 3591–3600.
[10] K. C. Holmes, et al., *Atomic model of the actin filament*, Nature, **347** (1990), 44–49.
[11] M. Karplus, Y. Q. Gao, J. Ma, A. van der Vaart and W. Yang, *Protein structural transitions and their functional role*, Phil. Trans. R. Soc. A, **363** (2005), 331–355.
[12] H. Kojima, A.Ishijima and T.Yanagida, *Direct measurements of stiffness of single actin filaments with and without tropomyosin by in vitro nanomanipulation*, Proc. Natl. Acad. Sci. USA, **91** (1994), 12962–12966.
[13] A. Lader, H. Woodward, E. Lin and H. Cantiello, *Modeling of ionic waves along actin filaments by discrete electrical transmission lines*, METMBS'00 International Conference, (2000), 77–82.
[14] E. Lin and H. Cantiello, *A novel method to study the electrodynamic behavior of actin filaments. Evidence for cable-like properties of actin*, Biophys. J., **65** (1993), 1371–1378.
[15] X. Liu and H. Pollack, *Mechanics of F-actin characterized with microfabricated cantilevers*, Biophys. J., **83** (2002), 2705–2715.
[16] T. Odijk, *Stiff chains and filaments under tension*, Macromolecules, **28** (1995), 7016–7018.
[17] A. Orlova and E. H. Egelman, *F-actin retains a memory of angular order*, Biophys. J., **78** (2000), 2180–2185.
[18] S. M. Perepelytsya and S. N. Volkov, *Counterion vibrations in the DNA low-frequency spectra*, Eur. Phys. J. E., **24** (2007), 261–269.
[19] M. Peyrard, *Nonlinear dynamics and statistical physics of DNA*, Nonlinearity, **17** (2004), R1–R40.
[20] M. Peyrard, S. Cuesta-López and G. James, *Nonlinear analysis of the dynamics of DNA breathing*, Journal of Biological Physics, **35** (2009), 73–89.
[21] S. Portet, C. Hogue, J. A. Tuszyński and J. M. Dixon, *Elastic vibrations in seamless microtubules*, European Biophysics Journal, **34** (2005), 912–920.
[22] A. Priel, A. J. Ramos, J. A. Tuszyński and H. F. Cantiello, *A biopolymer transistor: Electrical amplification by microtubules*, Biophys. J., **90** (2006), 4639–4643.
[23] A. Priel and J. A. Tuszyński, *A nonlinear cable-like model of amplified ionic wave propagation along microtubules*, EPL, **83** (2008), 68004.
[24] M. Salerno and Y. S. Kivshar, *DNA promoters and nonlinear dynamics*, Phys. Lett. A, **193** (1994), 263–266.
[25] A. V. Savin, L. I. Manevich, P. L. Christiansen and A. V. Zolotaryuk, *Nonlinear dynamics of zigzag molecular chains*, Physics-Uspekhi, **42** (1999), 245–260.
[26] J. A. Tuszyński, S. Portet, J. M. Dixon, C. Luxford and H. F. Cantiello, *Ionic wave propagation along actin filaments*, Biophys. J., **86** (2004), 1890–1903.
[27] L. V. Yakushevich, A. V. Savin and L. I. Manevitch, *Nonlinear dynamics of topological solitons in DNA*, Phys. Rev. E, **66** (2002), 016614.
[28] A. V. Zolotaryuk, P. L. Christiansen and A. V.Savin, *Two-dimensional dynamics of a free molecular chain with a secondary structure*, Phys. Rev. E, **54** (1996), 3881–3894.

E-mail address: cynthiaf@gmail.com
E-mail address: guillaume.james@imag.fr
E-mail address: Michel.Peyrard@ens-lyon.fr